

Signal-signal beat interference cancellation in spectrally-efficient WDM direct-detection Nyquist-pulse-shaped 16-QAM subcarrier modulation

Zhe Li,^{1,*} M. Sezer, Erkiñç,¹ Stephan Pachnicke,² Helmut Griesser,³ Rachid Bouziane,¹ Benn C. Thomsen,¹ Polina Bayvel,¹ and Robert I. Killey¹

¹Optical Networks Group, Department of Electronic and Electrical Engineering, University College London, Torrington Place, London, WC1E 7JE, UK

²ADVA Optical Networking SE, Maerzenquelle 1-3, 98617 Meiningen, Germany

³ADVA Optical Networking SE, Fraunhoferstr. 9a, 82152 Martinsried, Germany
[*zhe.li@ee.ucl.ac.uk](mailto:zhe.li@ee.ucl.ac.uk)

Abstract: An experimental demonstration of direct-detection single-sideband Nyquist-pulse-shaped 16-QAM subcarrier modulated (Nyquist-SCM) transmission implementing a receiver-based signal-signal beat interference (SSBI) cancellation technique is described. The performance improvement with SSBI mitigation, which compensates for the nonlinear distortion caused by square-law detection, was quantified by simulations and experiments for a 7×25 Gb/s WDM Nyquist-SCM signal with a net optical information spectral density (ISD) of 2.0 (b/s)/Hz. A reduction of 3.6 dB in the back-to-back required OSNR at the HD-FEC threshold was achieved. The resulting reductions in BER in single channel and WDM transmission over distances of up to 800 km of uncompensated standard single-mode fiber (SSMF) achieved are presented.

©2015 Optical Society of America

OCIS codes: (060.0060) Fiber optics and optical communications; (060.2360) Fiber optics links and subsystems.

References and links

1. Alcatel-Lucent, "Bell labs metro network traffic growth: architecture impact study," Strategic White Paper (2013).
2. Cisco, "Cisco visual networking index: forecast and methodology, 2013-2018," (2014).
3. S. Chandrasekhar, X. Liu, B. Zhu, and D. W. Peckham, "Transmission of a 1.2-Tb/s 24-carrier no-guard-interval coherent OFDM superchannel over 7200-km of ultra-large-area fiber," in *European Conference and Exhibition on Optical Communication (ECOC, 2009)*, paper 1.2.
4. J.-X. Cai, Y. Sun, H. G. Batshon, M. Mazurczyk, H. Zhang, D. G. Foursa, and A. N. Pilipetskii, "54 Tb/s transmission over 9,150 km with optimized hybrid Raman-EDFA amplification and coded modulation," in *European Conference and Exhibition on Optical Communication (ECOC, 2014)*, paper PD.3.3.
5. J. Zhang, J. Yu, Y. Fang, and N. Chi, "High speed all optical Nyquist signal generation and full-band coherent detection," *Sci. Rep.* **4**, 6156 (2014).
6. S. Beppu, M. Yoshida, K. Kasai, and M. Nakazawa, "2048 QAM (66 Gbit/s) single-carrier coherent optical transmission over 150 km with a potential SE of 15.3 bit/s/Hz," in *Optical Fiber Communication Conference, OSA Technical Digest Series (CD) (OSA, 2014)*, paper W1A.6.
7. T. J. Xia, S. Gringeri, and M. Tomizawa, "High-capacity optical transport networks," *IEEE Commun. Mag.* **50**(11), 170–178 (2012).
8. ADVA, Efficient 100G Transport (2014). <http://www.advaoptical.com/en/innovation/100g-transport.aspx>.
9. A. O. Wiberg, B.-E. Olsson, and P. A. Andrekson, "Single cycle subcarrier modulation," in *Optical Fiber Communication Conference, OSA Technical Digest Series (CD) (OSA, 2009)*, paper OTuE.1.
10. A. S. Karar and J. C. Cartledge, "Generation and detection of a 56 Gb/s signal using a DML and half-cycle 16-QAM Nyquist-SCM," *IEEE Photonics Technol. Lett.* **25**(8), 757–760 (2013).
11. M. S. Erkiñç, S. Kilmurray, R. Maher, M. Paskov, R. Bouziane, S. Pachnicke, H. Griesser, B. C. Thomsen, P. Bayvel, and R. I. Killey, "Nyquist-shaped dispersion-precompensated subcarrier modulation with direct detection for spectrally-efficient WDM transmission," *Opt. Express* **22**(8), 9420–9431 (2014).

12. M. S. Erkilinc, S. Pachnicke, H. Griesser, B. C. Thomsen, P. Bayvel, and R. I. Killey, "Performance comparison of single sideband direct-detection Nyquist-subcarrier modulation and OFDM," *J. Lightwave Technol.* **33**(10), 2038–2046 (2015).
13. A. J. Lowery, "Amplified-spontaneous noise limit of optical OFDM lightwave systems," *Opt. Express* **16**(2), 860–865 (2008).
14. S. A. Nezamalhosseni, L. R. Chen, Q. Zhuge, M. Malekiha, F. Marvasti, and D. V. Plant, "Theoretical and experimental investigation of direct detection optical OFDM transmission using beat interference cancellation receiver," *Opt. Express* **21**(13), 15237–15246 (2013).
15. J. Ma, "Simple signal-to-signal beat interference cancellation receiver based on balanced detection for a single-sideband optical OFDM signal with a reduced guard band," *Opt. Lett.* **38**(21), 4335–4338 (2013).
16. C. Sánchez, B. Ortega, and J. Capmany, "System performance enhancement with pre-distorted OOFDM signal waveforms in DM/DD systems," *Opt. Express* **22**(6), 7269–7283 (2014).
17. C. Ju, X. Chen, N. Liu, and L. Wang, "SSII cancellation in 40 Gbps VSB-IMDD OFDM system based on symbol pre-distortion," in *European Conference and Exhibition on Optical Communication (ECOC, 2014)*, paper P.7.9.
18. N. Liu, C. Ju, and X. Chen, "Nonlinear ISI cancellation in VSSB Nyquist-SCM system with symbol pre-distortion," *Opt. Commun.* **338**, 492–495 (2015).
19. W. R. Peng, X. Wu, K. M. Feng, V. R. Arbab, B. Shamee, J. Y. Yang, L. C. Christen, A. E. Willner, and S. Chi, "Spectrally efficient direct-detected OFDM transmission employing an iterative estimation and cancellation technique," *Opt. Express* **17**(11), 9099–9111 (2009).
20. H. Shi, P. Yang, C. Ju, X. Chen, J. Bei, and R. Hui, "SSBI cancellation based on time diversity reception in SSB-DD-OOFDM transmission systems," in *Conference on Lasers and Electro-optics (CLEO, 2014)*, paper JTh2A.14.
21. Z. Li, M. S. Erkilinc, S. Pachnicke, H. Griesser, B. C. Thomsen, P. Bayvel, and R. I. Killey, "Direct-detection 16-QAM Nyquist-shaped subcarrier modulation with SSBI mitigation," in *Proceedings of IEEE International Conference on Communications (ICC, 2015)*, to be published.
22. X. Zhang, J. Li, and Z. Li, "SSBI cancellation method for IMDD-OFDM System with a single photodiode," in *Progress In Electromagnetics Research Symposium (PIERS 2014)*, pp. 2719.
23. H. Bülow, F. Buchali, and A. Klekamp, "Electronic dispersion compensation," *J. Lightwave Technol.* **26**(1), 158–167 (2008).
24. R. I. Killey, P. M. Watts, V. Mikhailov, M. Glick, and P. Bayvel, "Electronic dispersion compensation by signal predistortion using digital processing and a dual-drive Mach-Zehnder modulator," *IEEE Photonics Technol. Lett.* **17**(3), 714–716 (2005).
25. M. S. Erkilinc, Z. Li, S. Pachnicke, H. Griesser, B. C. Thomsen, P. Bayvel, and R. I. Killey, "Spectrally-efficient WDM Nyquist pulse-shaped 16-QAM subcarrier modulation transmission with direct detection," *J. Lightwave Technol.* **33**(15), 3147–3155 (2015).
26. G. P. Agrawal, *Applications of Nonlinear Fiber Optics*, 3rd ed. (Academic, 2010).
27. C. E. Shannon, "A mathematical theory of communication," *Bell Syst. Tech. J.* **27**(3), 379–423 (1948).

1. Introduction

There is a continuously increasing demand for high bandwidth transmission due to data intensive services such as IP video, scientific and cloud computing, requiring low-cost and spectrally-efficient optical transmission systems in access, metropolitan and regional optical links [1, 2]. As a result, multi-level and multi-dimensional modulation techniques, such as quadrature amplitude modulation (QAM) in which the data is modulated on both amplitude and phase dimensions, have attracted much research interest in the last decade. Optical links utilizing coherent receivers enable the highest bit rates with the highest information spectral densities [3–7], but require complex transceiver hardware. In contrast, direct-detection (DD) optical links use a simpler receiver structure consisting of a single-ended photodiode and a single analogue-to-digital converter (ADC), and hence may be favorable for short- and medium-haul links (<500km). Service providers have recently started using 100 Gb/s metro solutions based on 4×28 Gb/s using direct detection technology and cost-effectiveness is the primary requirement in such links [8].

Nyquist-pulse-shaped subcarrier modulation was proposed in [9, 10]. It has been shown that single-sideband (SSB) Nyquist-SCM with direct detection is a promising and practical spectrally-efficient modulation technique for metro and access networks [11]. A QAM signal is filtered using Nyquist pulse shaping, and then modulated onto a single subcarrier. The generated pass-band (up-converted) signal is transmitted together with an optical carrier and is detected by a single-ended photodiode. The schematic diagram of the direct-detection system architecture considered in this paper is shown in Fig. 1. For direct-detection links, the optical phase of the transmitted signal is lost after square-law photodetection. However, if the

SCM technique is performed, both the amplitude and phase information of the subcarrier can be recovered after direct detection from the beating between optical carrier and subcarrier signal. In order to maximize the spectral efficiency, high-order QAM encoding, Nyquist pulse shaping, a subcarrier frequency lower than the symbol rate and digital sideband filtering to generate a SSB signal are all implemented. An advantage of the Nyquist-SCM technique, in comparison to other SCM formats such as optical orthogonal frequency division multiplexing (OFDM) which uses multiple orthogonal subcarriers, is its lower peak-to-average power ratio (PAPR), offering a lower optimum carrier-to-signal power ratio (CSPR). Hence, Nyquist-SCM requires a lower optical signal-to-noise ratio (OSNR) and has improved transmission performance [12].

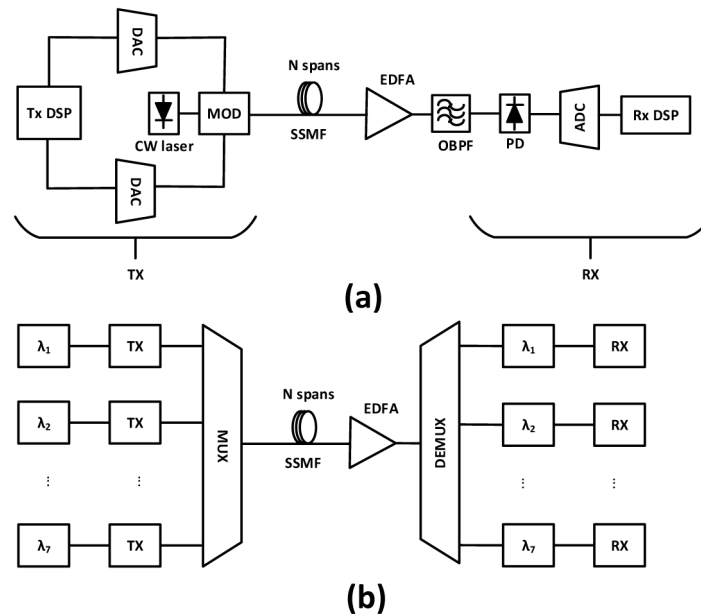


Fig. 1. System architecture for (a) single channel and (b) WDM transmission system.

A drawback of the direct-detection SCM technique (both Nyquist-SCM and OFDM) is that the signal-signal beat products interfere with the desired signal-carrier beat terms. This effect is known as signal-signal beat interference (SSBI) and causes a significant degradation in receiver sensitivity [13]. Therefore, it is desirable to develop effective compensation techniques to cancel or mitigate SSBI, and consequently, improve the performance of direct-detection SCM transmission systems.

Recently, a number of SSBI compensation techniques have been investigated for optical OFDM systems, including the use of an optical balanced receiver [14, 15], digital pre-distortion [16–18] or digital post-compensation [19–22] schemes. A drawback of the optical scheme is the resulting increased complexity of the receiver optical hardware such as implementing a balanced receiver which includes two photodiodes. On the other hand, the use of digital pre-distortion leads to an increased PAPR and imperfect SSBI mitigation introduced by extra beat products after square-law detection. Therefore, in this paper, we focus on the receiver-based digital compensation (post-compensation) technique, which offers good performance as well as simple optical hardware complexity.

We experimentally demonstrate the improvement in system margin gained using a receiver-based iterative digital SSBI estimation and cancellation technique on a direct detection dispersion pre-compensated SSB Nyquist-pulse-shaped 16-QAM SCM signal. The transmission performance of both a single channel and a 12-GHz spaced wavelength division multiplexed (WDM) system, operating at a bit rate of 25 Gb/s (net bit rate of 24 Gb/s) per

channel, with a net optical ISD of 2.0 (b/s)/Hz, was assessed. The receiver included only one single-ended photodiode and a single ADC. In optical back-to-back operation, the use of SSBI compensation led to reductions of the required OSNR at the hard-decision forward-error-correction (HD-FEC) threshold, and decreased bit-error ratio (BER) values after transmission over uncompensated standard single-mode fiber (SSMF).

2. Principles of operation

2.1. Single-sideband (SSB) Nyquist-pulse-shaped QAM subcarrier modulation

The generation process of SSB QAM Nyquist-SCM signaling is shown in Fig. 2(a). In order to reduce the spectral width of the signal, digital root-raised-cosine (RRC) filters are applied to the in-phase (I) and quadrature (Q) components of the baseband QAM signal to perform Nyquist pulse shaping. Then the filtered I- and Q-components are up-converted to an RF-subcarrier frequency (f_{sc}) and added to each other to generate a double sideband (DSB) Nyquist-SCM signal. A digital sideband filter is applied to remove the lower frequency sideband and, by biasing the optical modulator, an optical carrier is transmitted along with the sideband. The optical SSB QAM Nyquist-SCM signal spectrum is shown schematically in Fig. 2(b).

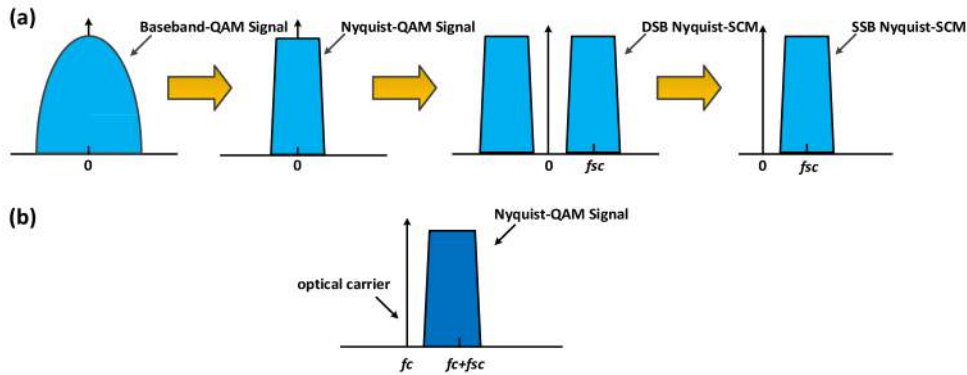


Fig. 2. Schematics of SSB QAM Nyquist-SCM signal generation: (a) Digital signal spectra (RRC filtering), up-conversion to the subcarrier frequency and sideband filtering. (b) Resulting optical signal spectrum.

2.2. Dispersion pre-compensation

A key attribute of the transceiver in optical fiber communication systems is its tolerance to fiber chromatic dispersion (CD). In direct-detection systems, the effect of chromatic dispersion, which is a linear distortion in the optical domain, is transformed into a nonlinear one in the electrical domain. Thus, it will lead to additional penalties, if receiver-based digital equalization is carried out [23]. Therefore, an effective approach to mitigate the dispersion accumulated along the transmission involves pre-distorting the signal at the transmitter, a technique termed electronic pre-distortion (EPD). As described in [24], the spectrum of the pre-distorted signal is written as:

$$E(\omega, 0) = E(\omega, L)H^{-1}(\omega) = E(\omega, L)\exp\left(j\frac{D}{4\pi c}\lambda^2\omega^2L\right)$$

where $E(\omega, L)$ is the signal before EPD, $H^{-1}(\omega)$ is the inverse of the channel response due to the chromatic dispersion, ω is the angular frequency, L is the total fiber transmission distance, λ is the wavelength, c is the speed of light in vacuum and D is the dispersion parameter.

2.3. Signal-signal beat interference (SSBI) iterative estimation and cancellation technique

A receiver-based iterative decision SSBI compensation technique has been previously proposed and investigated for direct-detection virtual SSB optical OFDM (VSSB-OOFDM) systems [19]. Here, we apply this concept to, and further refine the algorithm for, the SSB QAM Nyquist-SCM system, as shown in Fig. 3.

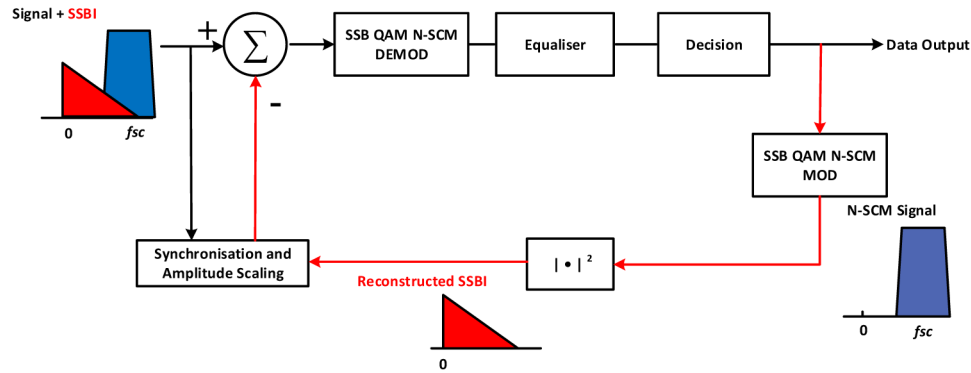


Fig. 3. Iterative decision SSBI cancellation technique [21].

The operation of the SSBI cancellation technique can be described as follows: (a) The detected signal waveform, which includes both the desired signal (signal-carrier beat products) and the unwanted signal-signal beat products, is stored in memory, and then frequency down-conversion, matched Nyquist-pulse-shaped filtering and equalization stages are applied to the detected signal; (b) after making symbol decisions, a digital representation of the ideal Nyquist-pulse-shaped 16-QAM SCM signal, with the received symbol sequence, is re-generated, and an approximation of the waveform of the signal-signal beat products is obtained by implementing the square-law detection process on this ideal re-generated signal without the optical carrier; (c) in order to achieve an accurate synchronization between the stored received signal waveforms and the waveform of the reconstructed signal-signal beat products, correlation calculations are carried out to determine the correct delay and amplitude scaling of the reconstructed signal-signal beat waveform, which is then subtracted from the stored received signal to partially eliminate the SSBI; (d) this compensation process is iteratively repeated. In contrast to the previously demonstrated SSBI post-compensation technique [19] which needs specially designed training symbols, no training sequence is required in this algorithm, only correlation calculations are sufficient for accurate synchronization. For all simulations and experiments described in this paper, the number of iterations was set to four, since no further significant OSNR gains were obtained with more iterations.

In direct-detection single-sideband optical communication systems, there is a trade-off between the SSBI and the signal-amplified spontaneous emission (ASE) beat noise. Signals with lower carrier-to-signal power ratio suffer from high SSBI, while high CSPR leads to large signal-ASE beat noise penalties. Hence, it is necessary to ensure that the system is operating at the optimum CSPR value. However, after SSBI compensation, the trade-off is changed (due to the lower impact of SSBI), therefore the CSPR value needs to be reduced to the new, lower optimum value to maximize the performance of SSBI compensation technique.

3. Experimental setup

As shown in Fig. 4, the optical transmission test-bed includes a 7×25 Gb/s SSB Nyquist-pulse-shaped 16-QAM SCM transmitter, an optical fiber recirculating loop and a direct-detection receiver for the channel of interest after demultiplexing. Within the transmitter, each IQ-modulator was driven by two field programmable gate arrays (FPGAs) interfaced to high

speed digital-to-analogue converters (Xilinx Virtex-5 FPGA and Micram VEGA DACII), with a DAC nominal resolution of 6 bits (the effective number of bits (ENOB) at 10 GHz is 3.5 bits) and sampling rate of 25 GSa/s. Electrical anti-imaging filters (5th-order Bessel LPFs) with a 7 GHz bandwidth were utilized to avoid linear crosstalk between WDM channels due to the images generated by the DACs. We used MATLAB to generate the I- and Q-components of the SSB Nyquist-pulse-shaped 16-QAM SCM signals offline and they were uploaded to the FPGA's random access memory (RAM) to serve as the driving signals for the IQ-modulators. Figure 5(a) shows the transmitter DSP design schematically. 2^{15} de Bruijn bit sequences decorrelated by 0.25 of the pattern length were used for the generation of a 16-QAM signal with 25 Gb/s (a symbol rate (f_s) of 6.25 GBaud). Nyquist pulse shaping was carried out on the I- and Q-components of the signal by a pair of RRC filters with a roll-off factor of 0.3, using 512-tap FIR filters with a stop-band attenuation of 40 dB. The Nyquist-pulse-shaped I- and Q-components were up-converted to a subcarrier frequency of 4.68 GHz ($f_{sc} = 0.75 \cdot f_s$) and added to each other to obtain a DSB Nyquist-pulse-shaped SCM signal. Following this, the DSB to SSB conversion was performed by applying a digital Hilbert transform filter to remove the lower frequency sideband. Finally, EPD was applied to compensate for the accumulated chromatic dispersion.

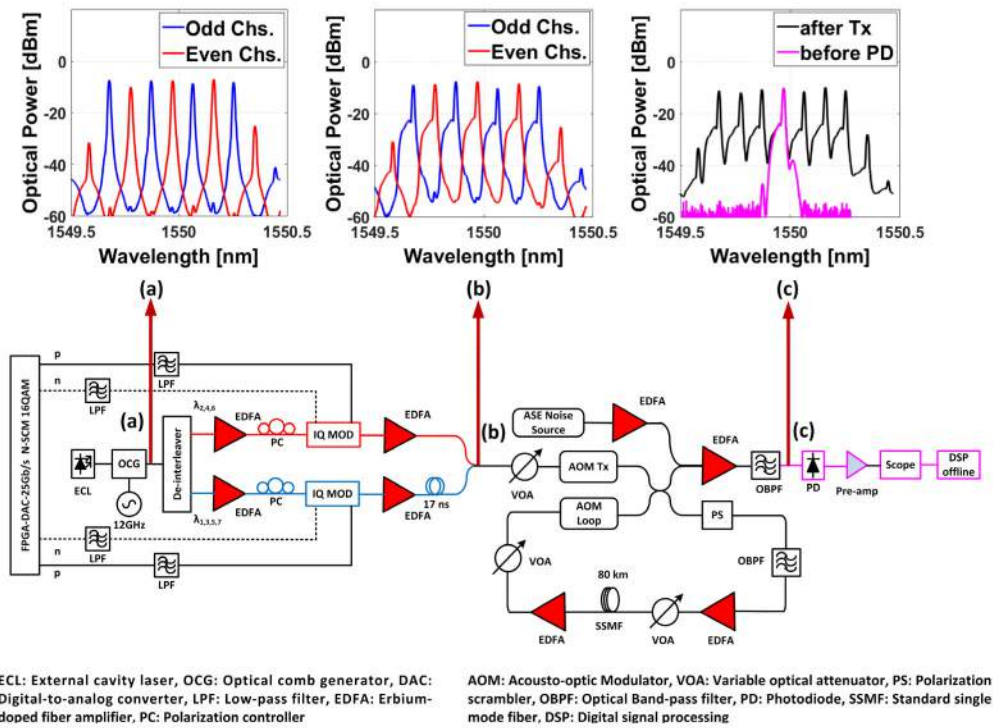


Fig. 4. Experimental setup for SSB 16QAM Nyquist-SCM transmission. Inset: Experimental spectra for WDM signal. (a) after OCG, (b) after transmitter and (c) transmitted and received signal.

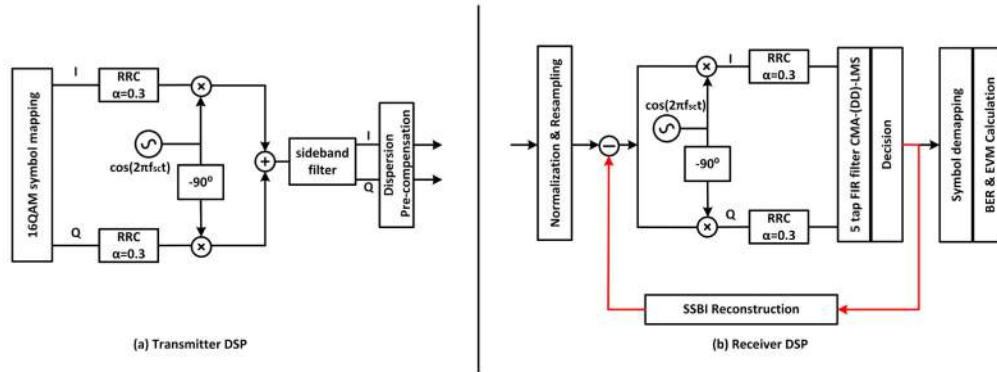


Fig. 5. (a) Transmitter and (b) receiver DSP design. CMA: Constant modulus algorithm. DD: Decision-directed. LMS: Least mean squares.

An external cavity laser (ECL) with a linewidth of 100 kHz at 1550 nm was used as a laser source for the optical comb generator (OCG), which consisted of cascaded optical amplitude and phase modulators which were overdriven by a 12 GHz clock signal for the generation of 7×12 GHz-spaced unmodulated optical channels, as shown in the inset (a) of Fig. 4. We utilized an ECL as a laser source due to its availability, though a laser source with larger linewidth can be employed in the direct-detection system. The channel spacing was carefully selected to ensure that the linear crosstalk penalty caused by neighboring channels was less than 1 dB. Klyia de-interleavers with a suppression ratio of 40 dB were used to separate the odd ($\lambda_{1, 3, 5, 7}$) and even ($\lambda_{2, 4, 6}$) channels to allow independent data encoding with uncorrelated bit sequences. Then the optical SSB Nyquist-pulse-shaped 16-QAM SCM signals were imposed on the spectral lines by the IQ-modulators. In order to achieve approximately linear mapping from the electrical to optical domain with the desired optical power, the optical carriers were added by biasing the optical modulators close to their quadrature points. The odd and even arms were amplified to 18 dBm and one arm was delayed by 17 ns (approximately 425 samples) using a decorrelating fiber before the WDM signal was launched into the recirculating loop. The optical spectra, measured with an optical spectrum analyzer (OSA) at a resolution of 0.01 nm, are shown in the inset (b) of Fig. 4. The peaks and asymmetric shapes of the optical spectra show the optical carriers and single-sideband signals respectively.

The transmission experiments were carried out using an optical recirculating fiber loop consisting of a single span of 80 km SSMF. A variable optical attenuator (VOA) was employed to control the launch power into the fiber loop and the other VOA was used to balance the optical power in the loop. The dispersion parameter at reference wavelength (D), fiber attenuation (α), nonlinear parameter (γ) and fiber length per span (L_{span}) were 17 ps/(nm·km), 0.2 dB/km, 1.2 / (W·km) and 80 km respectively. The total loss of 31 dB within the loop (16 dB fiber loss plus the combined losses due to the loop components (15 dB)) was compensated by two erbium-doped fiber amplifiers (EDFA) with a noise figure of 5 dB, which were operated in saturation mode (18 dBm output power). Further details of the experimental setup are given in [25].

At the receiver side, an optical bandpass filter (Yenista Optics XTM50-Ultrafine) with an adjustable bandwidth and a filter edge gradient of 800 dB/nm was used to demultiplex the channel of interest, as shown in Fig. 4(c). Note that the 3 dB bandwidth of the filter was tuned manually to 11 GHz, which enabled the optimum system performance. Following detection by a single-ended PIN photodiode, the detected electrical signal was pre-amplified and digitized by a single ADC (Tektronix DPO 72004 oscilloscope) at 50 GSa/s with an electrical bandwidth of 16 GHz and a nominal resolution of 8 bits (ENOB of 5 bits at 10 GHz). After normalization, the received signal was resampled to 2 samples per symbol. Down-conversion to baseband and matched filtering with a RRC filter (roll-off factor (α) of 0.3) were performed

as described in Fig. 5(b). For symbol re-timing, initially, a 5-tap constant modulus algorithm least mean square (CMA-LMS) finite impulse response (FIR) filter was applied for fast convergence, and the Viterbi-Viterbi algorithm was carried out for QAM phase correction before switching to decision-directed LMS mode. After making the 16-QAM hard decisions, the SSBI iterative compensator, described in section 2.3, was implemented, and, after four iterations, the signal was demodulated and the BER was calculated by error counting over 2^{18} bits.

4. Results and discussions

4.1. Single channel optical back-to-back performance

Simulations of an ideal 25 Gb/s direct-detection SSB Nyquist-pulse-shaped 16-QAM SCM system were carried out so that the potential system performance improvements could be assessed. Practical limiting parameters such as DAC/ADC quantization noise and electrical low-pass filtering effects were neglected, and an ideal rectangular (“brick-wall” shaped) optical band-pass filtering was assumed. The single channel optical back-to-back system performance (BER as a function of OSNR) was evaluated by ASE noise loading. It was important to optimize the CSPR for each OSNR value, individually for the cases with and without SSBI mitigation (since low CSPR leads to high SSBI penalties, and signals with high CSPR suffer from large signal-ASE beat noise). For the case of SSBI compensation, the optimum CSPR value was found to be 2 dB lower than the value without compensation, since the trade-off between the SSBI and signal-ASE beat noise is affected. The impact of the reduced optimum CSPR on the SSBI compensation technique will be discussed in detail in the following section. BER values versus OSNR (at a resolution of 0.1 nm), without and with SSBI compensation, are plotted in Fig. 6. It can be seen that the required OSNR at the 7% overhead HD-FEC threshold (assumed to be $\text{BER} = 3.8 \times 10^{-3}$) is found to be 20.7 dB without SSBI compensation, with an improvement by 4.2 dB to 16.5 dB for the case with SSBI compensation.

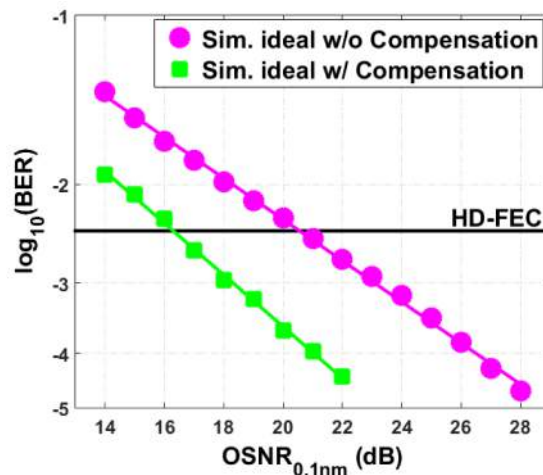


Fig. 6. Back-to-back BER versus OSNR in simulations considering ideal transceiver, without and with SSBI compensation.

Following the simulations of the ideal system, we carried out experiments to measure the system optical back-to-back performance. In the experiment, ASE noise loading at the receiver was performed to measure the BER versus OSNR. The CSPR value was swept from 5 dB to 10 dB and adjusted at each OSNR level to obtain the optimum system performance. The BER was measured and the resultant curves plotted as functions of OSNR for the cases without and with SSBI compensation are shown in Fig. 7(a). Additionally, simulations of the practical system were also performed for comparison, with the practical system parameters

(DAC/ADC quantization noise with an ENOB of 3.5 at 10 GHz, 5th-order Bessel electrical low-pass filtering with a 3 dB bandwidth of 7 GHz at the transmitter, and an 11 GHz 6th-order super-Gaussian OBPF at the receiver) taken into account. The practical simulation results match well with the experimental measurements. They indicate a 4 dB improvement in the required OSNR value at the HD-FEC threshold, similar to the experimental measurements, an improvement of 3.6 dB. The difference between experimental and simulation results can be partially explained by the imperfect adjustments of the CSPR values in the experiment.

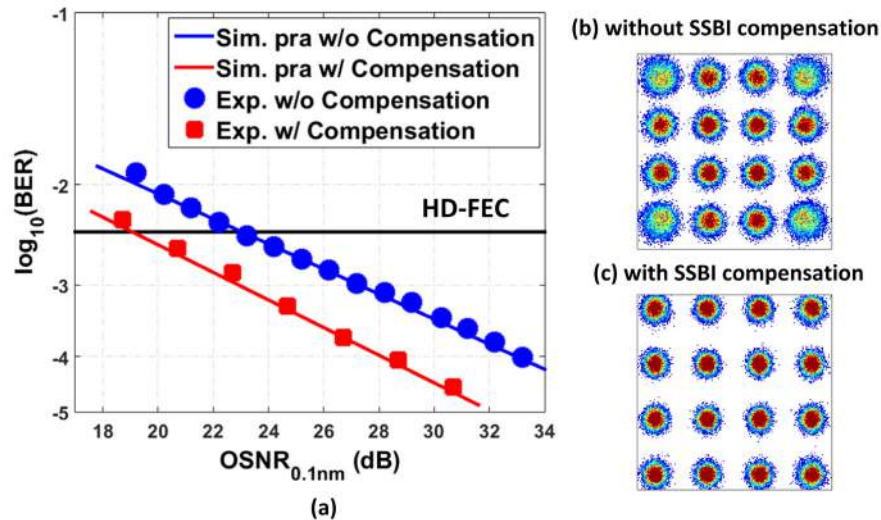


Fig. 7. (a) Simulated and experimental BER versus OSNR without and with SSBI compensation (left). Experimental back-to-back received constellation (right) at the OSNR of 30.3 dB, (b) without (EVM = 14.45%) and (c) with (EVM = 10.20%) SSBI compensation.

In order to observe the effect of SSBI compensation, the optical back-to-back signal constellations at a high OSNR value (30.3 dB), without and with SSBI compensation are plotted in Figs. 7(b) and 7(c). It can be observed that after SSBI compensation, the compensated constellation is significantly less distorted than the uncompensated one, especially in the four points in the corners, which are most affected by the SSBI due to their higher symbol energies. The error-vector-magnitude (EVM) decreased from 14.5% to 10.2% with SSBI compensation. Furthermore, the uncompensated and compensated received digital spectra at the same OSNR value are plotted in Fig. 8(a), together with the spectrum of the reconstructed SSB products, which were subtracted from the stored signal during SSBI compensation after synchronization and amplitude scaling, as shown in Fig. 8(b). Since some of the signal-signal beat terms exist within the spectral guard-band between the optical carrier and the sub-channel [13], the SSBI mitigation can be observed from the amplitude reduction (approximately 5 dB) within the guard-band.

As discussed in Section 2.3, the trade-off between the SSBI and signal-ASE beat noise, achieved through optimization of the carrier-to-signal power ratio, is affected when SSBI cancellation is performed. The CSPR was swept for different values of OSNR and the simulated and experimental BER curves, without and with compensation at 21 dB, 25 dB and 29 dB OSNR are plotted in Figs. 9(a)-9(c). A good match was found between the simulated and experimental results, and it can be seen that the optimum CSPR value is reduced by approximately 2 dB after applying SSBI compensation in each plot.

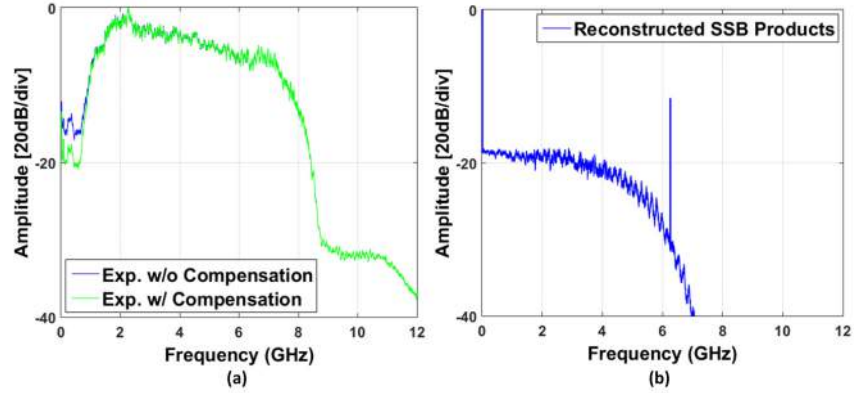


Fig. 8. Experimental back-to-back detected digital spectra at the OSNR of 30.3 dB, (a) without and with SSBI compensation and (b) reconstructed SSB.

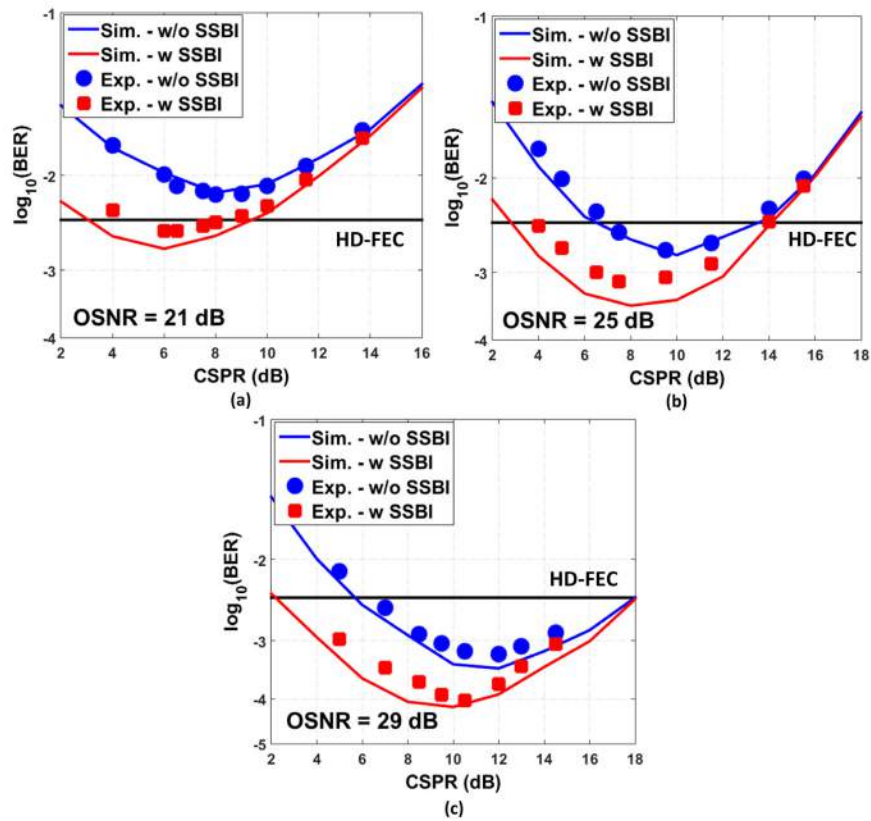


Fig. 9. Simulated and experimental BER versus CSRP without and with SSBI compensation at an OSNR of (a) 21 dB, (b) 25 dB, and (c) 29 dB in back-to-back operation.

The experimental BER curves as functions of CSRP at six different OSNR values, without and with SSBI compensation are plotted in Figs. 10(a) and 10(b), clearly exhibiting how SSBI compensation leads to improvements of the system BER performance, and reductions in the optimum CSRP value by approximately 2 dB. Figure 7 plots the BER as a function of OSNR at the optimum CSRP obtained from these results.

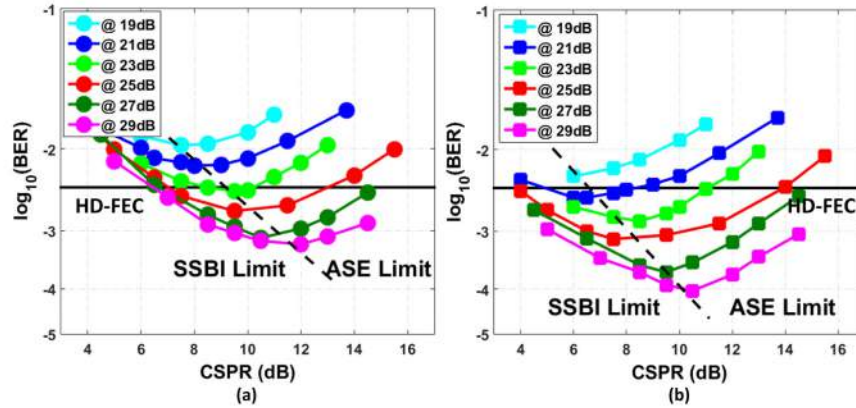


Fig. 10. Experimental BER versus CSPR at different OSNRs (a) without and (b) with SSBI compensation in back-to-back operation. The dashed black line indicates the shift in the optimum CSPR value.

The EVM versus the number of iterations of the SSBI compensation algorithm for a range of OSNR values are plotted in Fig. 11. It can be seen that at lower OSNR values, more iterations are required due to the inaccurate symbol decisions made after demodulation. In order to fully exploit the performance of the SSBI mitigation technique, we used four iterations for the following measurements.

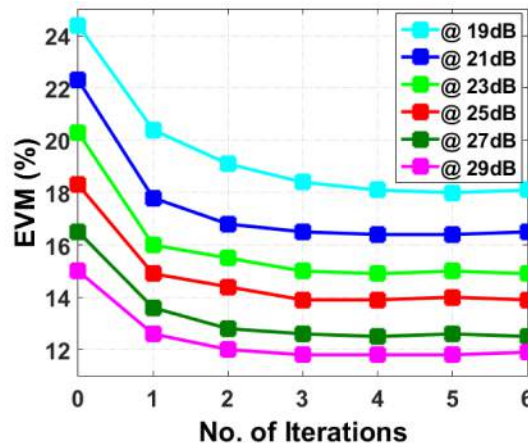


Fig. 11. Experimental EVM versus the receiver iteration numbers at different OSNRs.

4.2. Single channel transmission performance

After testing the optical back-to-back performance, single channel transmission experiments over 7 spans (560 km) and 10 spans (800 km) of SSMF using the 25 Gb/s SSB Nyquist-pulse-shaped 16-QAM SCM signal occupying an optical bandwidth of 8.75 GHz were carried out. These experiments were performed using the optical test-bed shown in Fig. 4, and the system performance, without and with SSBI compensation, was evaluated.

The system performance was characterized in terms of BER as the optical launch power was swept from -5 dBm to $+5$ dBm. For each launch power the optimum CSPR value was determined. To adjust the CSPR value, it is necessary to vary the bias voltages applied to the IQ modulator. In a practical implementation, the measurements of the pre-FEC BER would be fed back from the receiver to the transmitter, and the modulator bias voltages would be adjusted dynamically to minimise this BER. For 560 km transmission, shown in Figs. 12(a)-12(c), the optimum CSPR value was found to be 10 dB and optimum launch power was

approximately 1 dBm without SSBI compensation, while with SSBI compensation, the optimum launch power was reduced to -1 dBm and the optimum CSPR was reduced to 8 dB. The minimum BER at this launch power was improved from 3.0×10^{-3} to 7.9×10^{-4} , and the EVM was decreased from 17.6% to 14.2%. Furthermore, the range of launch powers at which the BER values were below the HD-FEC threshold was increased from approximately 3.5 dB to more than 8 dB. As can be observed from Figs. 13(a)-13(c), an approximately 2 dB reduction (from 1 dBm to -1 dBm) of the optimum launch power was obtained by utilizing SSBI compensation at 800 km. Moreover, the compensated BER at this launch power was improved from 5.3×10^{-3} to 1.7×10^{-3} and the EVM changed from 19.4% to 16.5%, enabling the system to exceed the HD-FEC limit required for error-free operation.

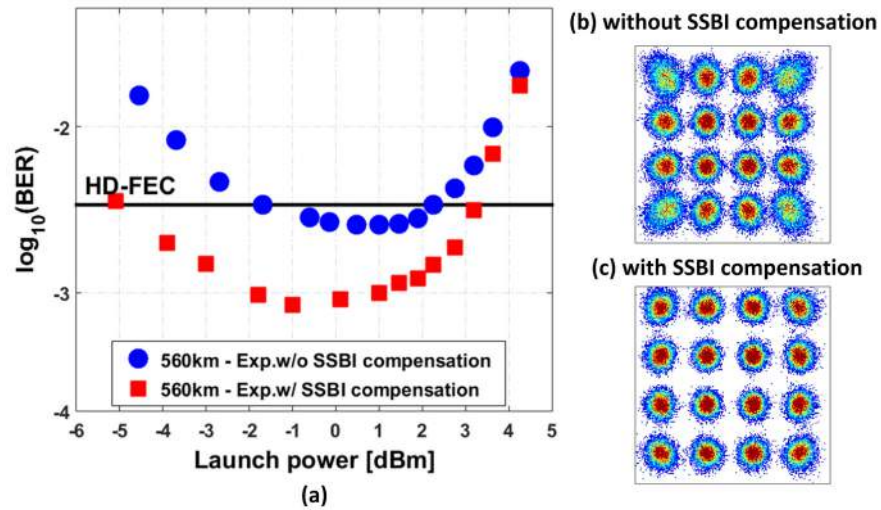


Fig. 12. (a) Experimental BER versus optical launch power for 560 km single channel transmission, without and with SSBI compensation (left) and experimental 560 km transmission received constellation (right) (b) without (EVM = 17.63%) and (c) with (EVM = 14.15%) SSBI compensation at the optimum launch power.

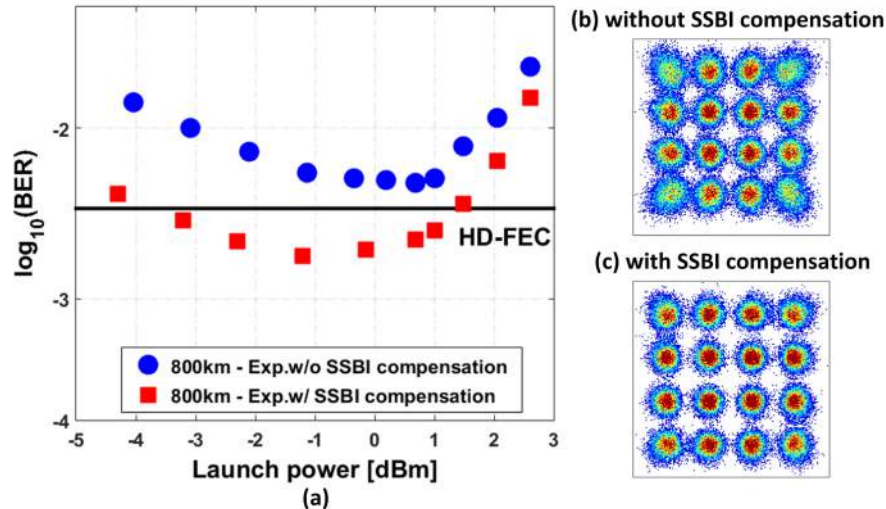


Fig. 13. (a) Experimental BER versus optical launch power for 800 km single channel transmission, without and with SSBI compensation (left) and experimental 800 km transmission received constellation (right) (b) without (EVM = 19.43%) and (c) with (EVM = 16.53%) SSBI compensation at the optimum launch power.

4.3. WDM transmission performance

Following the single channel transmission measurements, simulations and experiments investigating WDM transmission over 3 spans (240 km) and 4 spans (320 km) of SSMF were performed. To model the WDM transmission simulation, 7×12 GHz-spaced channels each carrying 25 Gb/s SSB Nyquist-pulse-shaped 16-QAM SCM signals were generated and the SSMF was modelled using the symmetric split-step Fourier method [26] to solve the nonlinear Schrödinger equation (NLSE). The experimental WDM system performance, without and with SSBI compensation, was measured using the optical test-bed shown in Fig. 4.

An additional 1 dB penalty due to the linear crosstalk caused by WDM neighboring channels was measured for the optical back-to-back performance compared to the single channel system in both practical simulation and experiment. In the transmission tests, the BER was measured for a range of optical launch powers, swept between -5 dBm and 3 dBm per channel, in each case operating with the optimized CSPR. The simulated and experimental BER curves as functions of optical launch power over 240 km and 320 km without and with SSBI compensation are plotted in Figs. 14 and 15. It can be observed that there is a very good agreement between the simulation and experimental results at both transmission distances.

For WDM transmission over 240 km, through the use of SSBI compensation, the optimum optical launch power was reduced from -0.5 dBm to -1.5 dBm per channel and the BER at the optimum launch power was decreased from 2.8×10^{-3} to 1.4×10^{-3} . The optimum CSPR value was found to be in the range of 8-9 dB. The launch power range resulting in BER values lower than the HD-FEC limit was increased from 4 dB to approximately 7 dB. At the transmission distance of 320 km, which was the transmission limit without compensation (BER = 3.7×10^{-3}), the use of SSBI compensation reduced the minimum BER to 1.9×10^{-3} and the optimum launch power was reduced from -1 dBm to -2 dBm. The launch power range for error free operation with HD-FEC was broadened to more than 5 dB.

If we compare the SSBI compensation effect of the single channel transmission with the 7 channel WDM transmission, we find the improvement in the 7 channel WDM system is less than that of the single channel system. This is mainly because, while the SSBI distortion is the dominant effect compared with the other penalties in the single channel system, in the case of

WDM transmission, the distortion due to fiber nonlinearity starts to dominate the performance so that SSBI becomes less significant. Despite this, receiver-based SSBI cancellation still provides increased margin for system operation.

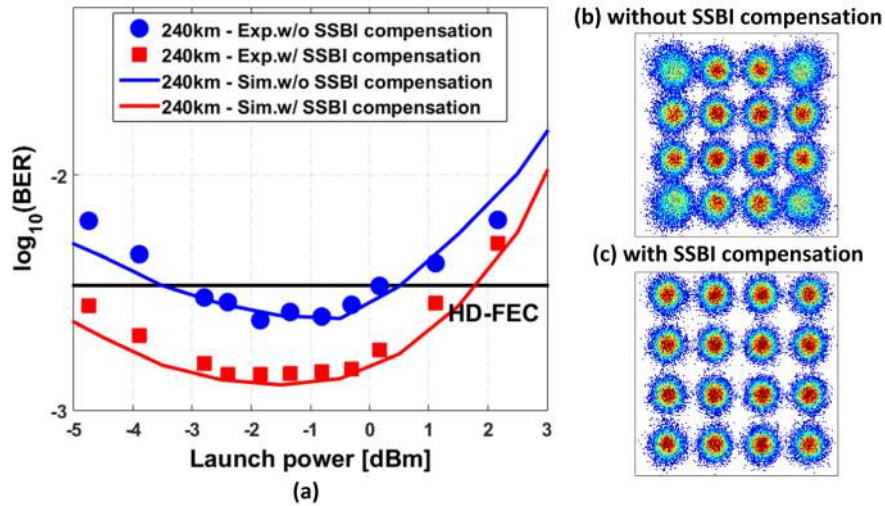


Fig. 14. (a) Simulated and experimental BER versus optical launch power per channel for 240 km WDM transmission, without and with SSBI compensation (left) and experimental 240 km transmission constellations (right) (b) without (EVM = 18.93%) and (c) with (EVM = 15.55%) SSBI compensation at the optimum launch power.

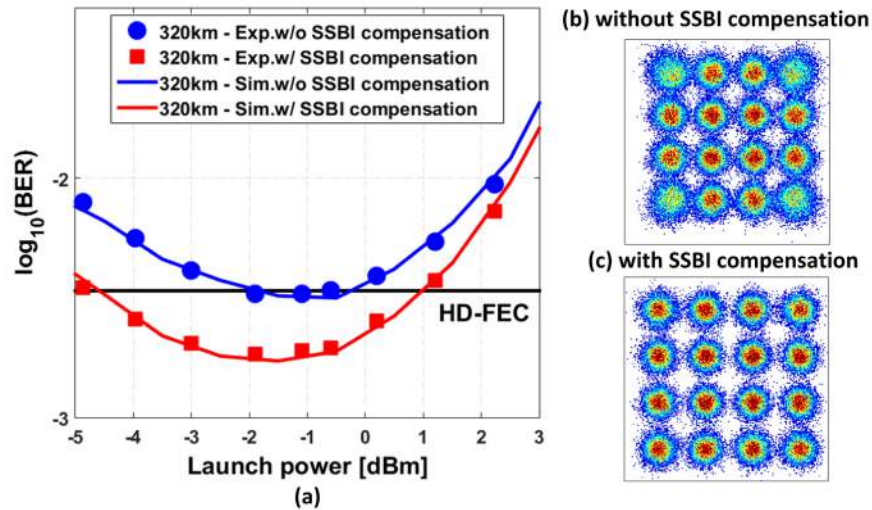


Fig. 15. (a) Simulated and experimental BER versus optical launch power per channel for 320 km WDM transmission, without and with SSBI compensation (left) and experimental 320 km transmission constellation (right) (b) without (EVM = 19.85%) and (c) with (EVM = 16.82%) SSBI compensation at optimum launch power.

For the case of WDM transmission over 320 km, the performance of all 7 channels was measured at the optimum launch power per channel, without and with SSBI compensation, with the results shown in Fig. 16. The net bit-rate per channel was calculated to be 24 Gb/s (a gross bit rate of 25 Gb/s) based on the theoretical hard decision decoding bound for the binary symmetric channel at a BER of 3.8×10^{-3} [27], and the optical net ISD was 2.0 b/s/Hz (a gross optical ISD of 2.08 b/s/Hz).

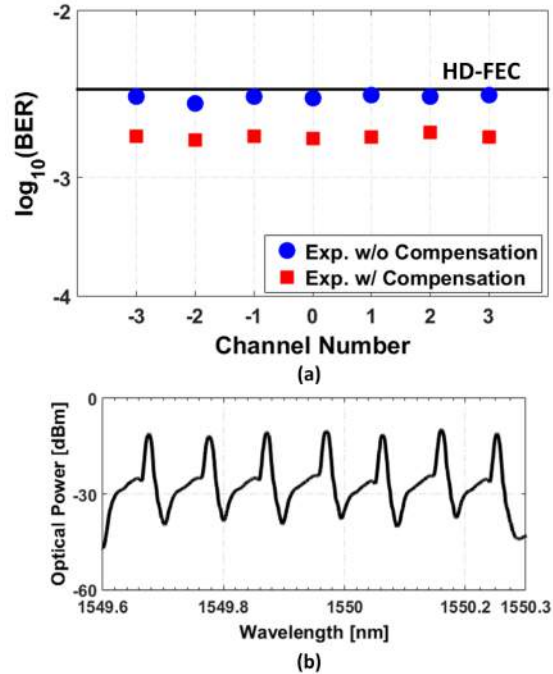


Fig. 16. (a) BER for each received channel over 320 km transmission without and with SSBI compensation. (b) Transmitted optical spectrum.

A drawback of the iterative compensation scheme is the additional complexity of the receiver DSP. This is mainly due to the inaccurate symbol decision which leads to the inaccurate estimation of the reconstructed signal-signal beat products. Further work is required to develop effective, low-complexity algorithms, for SSBI mitigation. The use of the guardband between the optical carrier and the sideband reduces the SSBI penalty for the case without compensation. However, the use of SSBI compensation allows the reduction of this guardband towards zero, with negligible effect on the performance. Hence, in our future work, we will assess the performance of SSBI compensation on Nyquist-SCM systems without a guardband.

5. Summary

The performance of single channel and WDM direct-detection single-sideband Nyquist-pulse-shaped 16-QAM subcarrier modulation system implementing both electronic chromatic dispersion pre-compensation and receiver-based signal-signal beat interference cancellation was experimentally demonstrated in transmission of 7×24 Gb/s channels with a net optical ISD of 2.0 b/s/Hz. The optical back-to-back operation and transmission performance without and with the application of the SSBI compensation technique were compared in both simulations and experiments. It was shown that the proposed SSBI compensation utilizes a very simple synchronization method without introducing any overhead and significantly reduces the penalty caused by nonlinear distortion due to square-law detection. Ideal simulations for back-to-back operation show a potential reduction in the required OSNR of 4.2 dB at the HD-FEC threshold, with experiments showing a 3.6 dB improvement. The performance gain through reducing the optimum carrier-to-signal power ratio (CSRP) value (approximately 2dB) to provide further system performance (1.4 dB gain on the required OSNR) was also experimentally confirmed. Following this, single channel and WDM transmission simulations and experiments were both carried out. Utilizing SSBI compensation, BER values were decreased from 3.0×10^{-3} to 7.9×10^{-4} and from 5.3×10^{-3} to 1.7×10^{-3} for single channel transmission over 560 km and 800 km respectively, with a 2

dB reduction in the optimum optical launch power. In the WDM case, the BER values were reduced from 2.8×10^{-3} to 1.4×10^{-3} and 3.7×10^{-3} to 1.9×10^{-3} for transmission over 240 km and 320 km respectively. The optimum optical launch power per channel was also decreased by approximately 1 dB. The results showed that the gain from SSBI compensation was reduced at the longer WDM transmission distances, because fibre nonlinearity started to dominate the system performance. To the best of our knowledge, this is the first experimental assessment of the use of SSBI cancellation in WDM Nyquist-pulse-shaped single subcarrier modulation systems, which offer high information spectral density and cost-effective transceiver design. Thus, it is a potentially attractive solution for low-cost, spectrally-efficient metro, regional and access links employing direct detection.

Acknowledgments

This work has been supported by the EU ERA-NET + project PIANO + IMPACT, UK EPSRC UNLOC project, EU FP7 ASTRON project and Semtech Corporation.